Current Optics and Photonics
Vol. 3, No. 2, April 2019, pp. 105-110

ISSN: 2508-7266(Print) / ISSN: 2508-7274(Online)
DOI: https://doi.org/10.3807/COPP.2019.3.2.105

Modeling Green-light Fiber Amplifiers for Visible-light Communication Systems

Muhammad Hanif Ahmed Khan Khushik and Chun Jiang*

State Key Laboratory of Advanced Optical Communication Systems and Networks, Shanghai Jiao Tong University, Shanghai 200240, China

(Received September 28, 2018 : revised November 29, 2018 : accepted January 28, 2019)

The visible-light communication (VLC) system is a promising candidate to fulfill the present and future demands for a high-speed, cost-effective, and larger-bandwidth communication system. VLC modulates the visible-light signals from solid-state LEDs to transmit data between transmitter and receiver, but the broadcasting and the line-of-sight propagation nature of visible-light signals make VLC a communication system with a limited operating range. We present a novel architecture to increase the operating range of VLC. In our proposed architecture, we guide the visible-light signals through the fiber and amplify the dissipated signals using visible-light fiber amplifiers (VLFAs), which are the most important and the novel devices needed for the proposed architecture of the VLC. Therefore, we design, analyze, and apply a VLFA to VLC, to overcome the inherent drawbacks of VLC. Numerical results show that under given constant conditions, the VLFA can amplify the signal up to 35.0 dB. We have analyzed the effects of fiber length, active ion concentration, pump power, and input signal power on the gain and the noise figure (NF).

Keywords : Visible light fiber amplifier, Visible light communication, Gain, Noise figure
OCIS codes : (060.1155) All-optical networks; (060.2310) Fiber optics; (060.4510) Optical communications; (060.2320) Fiber optics amplifiers and oscillators

I. INTRODUCTION

Visible light communication (VLC) can address interference, limited spectrum, safety, and high cost issues associated with traditional RF communication systems [1, 2]. Furthermore, the advent of solid-state lighting (SSL) technology and the use of high power LEDs for indoor and outdoor illumination, have paved the path for visible light communication (VLC) system to be used as the future communication system [3, 4]. VLC modulates visible light signals (400~700nm) from the LEDs used for illumination to transmit data between receiver and transmitter [5]. Although VLC is a green technology and is the best substitute for the existing RF systems. The need of line-of-sight and the broadcast nature of visible light signals (VLS) are the hindrances for the VLC to completely replace the RF systems. The broadcast nature of VLSs poses security issues, and the need for a line of sight limits the operating range of VLC [6, 7]. To extend the operating range and security of VLC is an ongoing challenge to optical engineers, scientists, and researchers. A spatial modulation technique was introduced to address the security issues caused by the broadcast nature of the VLS [6]. To address the shadowing effect produced by the line-of-sight propagation nature of the VLS, techniques such as employing receivers having a wide field of view (WFOV) [7] and shadowing ray-tracing algorithm (SRT) [8] were suggested. So far, no technique has been suggested to solve the security and line-of-sight problems of VLC simultaneously, according to the best of our knowledge.

In this paper, we propose a modern technique that can solve both inherent problems of VLC simultaneously, by making it more secure and extending its operating range. In our proposed technique, we guide visible-light signals through a fiber and use visible-light fiber amplifiers (VLFAs, novel devices) to amplify the dissipated signals. The VLFA is the most important and the novel device needed for our proposed technique; therefore, we model, analyze, and apply

*Corresponding author: cjiang@sjtu.edu.cn, ORCID 0000-0003-1873-6385
Color versions of one or more of the figures in this paper are available online.

VLFAs to VLC to address its fundamental drawbacks. We use erbium-doped silica glass to model a VLFA for the amplification of green light from the visible spectrum. The reasons for selecting green light to be used in visible-light communication systems include the facts that green light lies in the middle of the visible spectrum, so the human eye can perceive it clearly, and that green light is widely used for signaling in traffic, aviation, defense, hospitals, and many other applications. VLC utilizing green light for communication can be used in hospitals and in telemedicine because it presents no hazards to the eyes or the rest of the human body. Another important reason for choosing green light for use in VLC is the ability of erbium-doped silica glass to amplify green light, when pumped with cost-effective and easily available high-power semiconductor (Al,Ga)As laser diodes. Here we use erbium-doped silica glass to model VLFAs for VLC. The theoretical analysis of VLFAs, proposed architecture for VLC, and finally the conclusion is given in the following sections.

II. THEORETICAL MODEL OF THE VLFA

Figure 1 shows the energy levels of erbium in silica glass, and the radiative and non-radiative transitions involved in the amplification of green light [9]. Initially, all erbium ions are in the ground state. The co-directional pumping scheme is used to excite the ions to the upper lasing level. The excitation of the active ions is carried by the absorption of two pump photons. The ground-state absorption of the pump photons at a wavelength of 808 nm excites electrons from the ground level to $^4I_{9/2}$, from which they relax to the short-lived $^4I_{11/2}$ and the metastable level $^4I_{13/2}$ through multiphonon relaxation. In silica glass, the lifetime of the level $^4I_{9/2}$ is much smaller (around 10~20 μs) than in fluoride glasses (300 μs) [11]. The shorter lifetime of the $^4I_{9/2}$ level reduces the threshold pump power and helps to attain population inversion between upper and lower lasing levels; that is the reason why erbium-doped silica glass is best suited for the amplification of green light. All of the ions excited to $^4I_{9/2}$ relax to the metastable level $^4I_{13/2}$. The ions from $^4I_{13/2}$ are re-excited to the thermally coupled $^4S_{3/2}$ and $^2H_{11/2}$ states through excited-state absorption (ESA) of pump photons. The ground-state absorption (GSA) and ESA of pump photons around the 808-nm pumping band have been discussed extensively in the past, and strongly depend on the pump wavelength [10, 11]. In erbium-doped silica glasses, the ratio of ESA to GSA is higher than in fluoride glasses, which reduces the performance of devices at the 1530-nm band. The careful selection of pump wavelength can compensate the drawback of higher ESA to GSA ratio, and the advantage of a short lifetime of the $^4I_{9/2}$ level in silica glass can be utilized to obtain better amplification of green light. Here we use 808 nm as the pump wavelength, because the GSA and ESA of silica glass at this wavelength are almost equal. Equality of GSA and ESA can enhance the population inversion between upper and lower lasing levels.

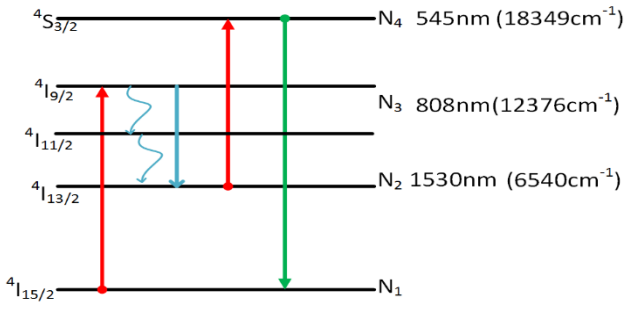

FIG. 1. The energy levels and lasing transitions of erbium ions in silica-glass fiber.

$$\frac{dN_1}{dt} = -(W_{13} + W_{14}) \times N_1 + A_{21} \times N_2 + (W_{31} + A_{31}) \times N_3 + (W_{41} + A_{41}) \times N_4 \quad (1)$$

$$\frac{dN_2}{dt} = -(W_{24} + A_{21}) \times N_2 + A_{32} \times N_3 \quad (2)$$

$$\frac{dN_3}{dt} = W_{13} \times N_1 - A_{32} \times N_3 - (W_{31} + A_{32} + A_{31}) \times N_3 \quad (3)$$

$$N_4 = N - N_1 - N_2 - N_3 \quad (4)$$

Equations (1)~(4) are the rate equations based on Fig. 1. In Equations (1)~(4), N_1, N_2, N_3, and N_4 are the numbers of erbium ions in the energy levels $^4I_{15/2}$, $^4I_{13/2}$, $^4I_{9/2}$, and $^4S_{3/2}$ respectively. N is the erbium ion concentration. A_{ij} represents the spontaneous decay rate of the excited ions from level i to level j. W_{ij} represents the transition rate from level i to level j. The transition rate can be given as [12]

$$Wij = \frac{P_k \sigma_{ij}(\lambda)}{A_{eff} h V_k} \quad (5)$$

where P_k is the pump or signal power, h is Planck's constant, V_k is the frequency, A_{eff} is the effective area of the doped fiber's core, and σ_{ij} (λ) is the emission or absorption cross section between levels i and j. The propagation equations, which involve the effective overlap factors rather than the integrals, are given below.

$$\frac{dP_{545}}{dz} = \Gamma_{545}(\sigma_{41} \times N_4 - \sigma_{14} \times N_1) \times P_{545} - \alpha_{545} \times P_{545} \quad (6)$$

$$\frac{dP_{808}}{dz} = \Gamma_{808}(\sigma_{31} \times N_3 - \sigma_{13} \times N_1 + \sigma_{42} \times N_4 - \sigma_{24} \times N_2) \times P_{808} - \alpha_{808} \times P_{808} \quad (7)$$

$$\frac{dP_{ASE}}{dz} = \Gamma_{545}(\sigma_{41} \times N_4 - \sigma_{14} \times N_1) \times P_{545} + 2 \times h \times \nu \times \Delta\nu \times \sigma_{41} \quad (8)$$

where Γ_λ is the overlap factor, which can be calculated as in [10],

$$\Gamma = \left(1 - e^{-R^2/\omega^2}\right) \quad (9)$$

where R is the radius of the fiber core and ω is the spot size, which also can be calculated as in [10],

$$\omega = \frac{1}{\sqrt{2}}\left(0.65 + \frac{1.619}{V^{1.5}} + \frac{2.879}{V^6}\right) V \quad (10)$$

where V is the fiber's V-number, a dimensionless number that determines the number of modes that can propagate through the fiber.

III. ANALYSIS OF VLFA

3.1. Gain Analysis

Table 1 contains the spectroscopic parameters used in the numerical analysis of the VLFA. Figure 2(a) shows that increasing pump power enhances the optimal length of the fiber amplifier, thereby increasing its gain. Pump powers of 100, 200, 300, 400, and 500 mW produce maximum gains of 7.5, 14.1, 22.5, 29.1, and 35.0 dB, if the length of the VLFA is kept at 1.2, 2, 2.8, 3.5, and 4.2 m respectively.

TABLE 1. The spectroscopic parameters used for the numerical analysis of green-light amplification

Parameter	Value	Unit	Remarks
σ_{13}	0.6×10^{-25}	m^2	[11, 13]
σ_{24}	0.65×10^{-25}	m^2	[11, 13]
σ_{14}	0.13×10^{-25}	m^2	[13]
σ_{41}	6.5×10^{-25}	m^2	[14]
A_{21}	71.4	s^{-1}	[14]
A_{32}	52.41	s^{-1}	[15]
A_{41}	274.7	s^{-1}	[16]
A_{31}	455	s^{-1}	[16]
A_{43}	172	s^{-1}	[16]
A_{42}	147	s^{-1}	[16]
Γ_{808}	0.976		
Γ_{545}	0.9		
Diameter	2.5	μm	

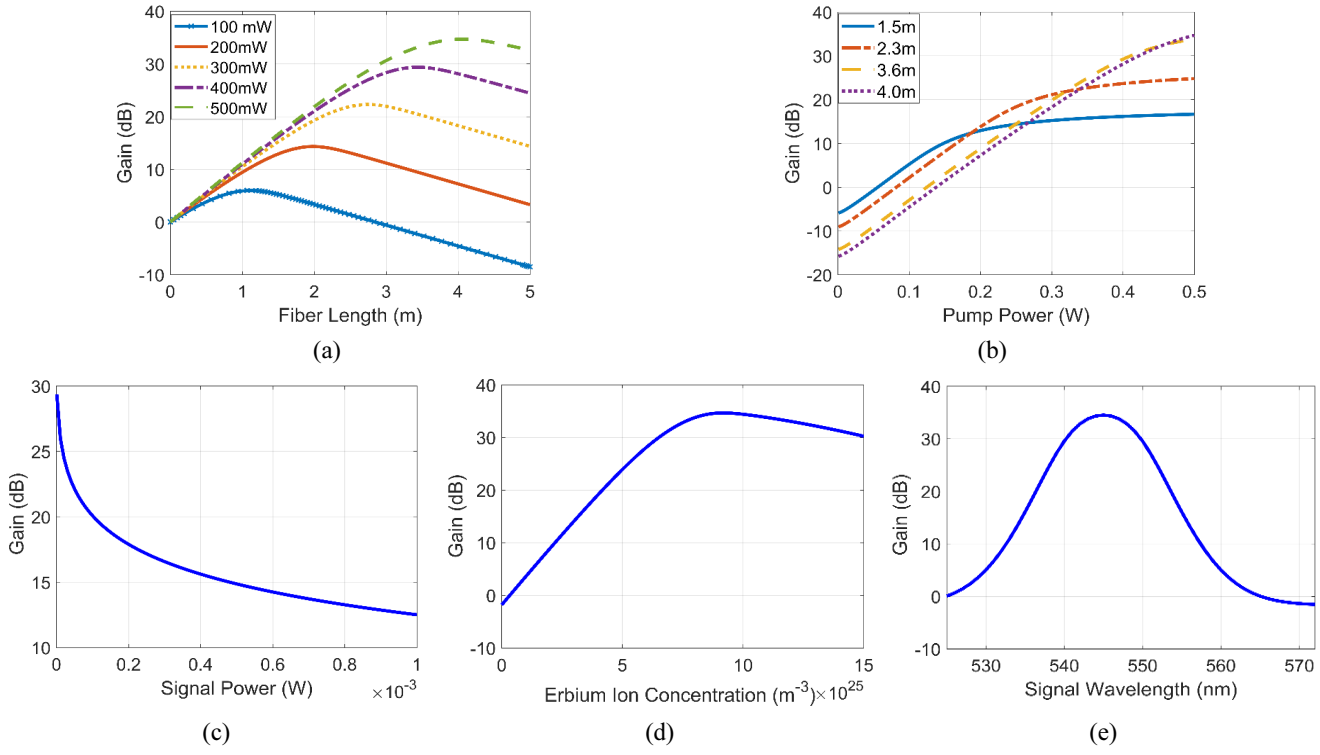

FIG. 2. The gain characteristics of the fiber amplifier: (a) gain as a function of fiber length for different pump powers, (b) gain as a function of pump power for different fiber lengths, (c) gain as a function of input signal power, (d) gain as a function of active-ion concentration, (e) gain as a function of signal wavelength.

The minimum pump power required for population inversion, *i.e.* $N \geq N_1$, or for zero gain, is known as the *threshold pump power*. The VLFA must be pumped with more than the threshold pump power to amplify the signal; pump power lower than the threshold power dissipates the signal, rather than amplifying it. The threshold pump power depends on several parameters, such as spectroscopic properties of the host glass, active ion concentration, and fiber length. Figure 2(b) explains the gain characteristics of the VLFA with varying pump power for different fiber lengths. This figure shows that for amplifier lengths of 1.5, 2.3, 3.6, and 4.0 m the threshold pump power is approximately 63, 79, 121, and 130 mW respectively. Figure 2(b) also indicates that to achieve maximum gains of 12.3, 21.7, 32.01, and 35.0 dB from a 1.5, 2.3, 3.6, and 4.0 m -long amplifier, pumping at 220, 300, 400, and 500 mW respectively is sufficient.

The increasing input signal power causes the amplifier to saturate, thereby reducing the gain of the amplifier. The variation of gain as a function of input signal power at constant pump power of 400 mW, erbium concentration of 9×10^{25} ions/m^3, and fiber length of 3.5 m is shown in Fig. 2(c). This shows that as the input signal power increases from 1 μW to 1 mW, the gain decreases from around 29.0 dB to 12.7 dB. The decreasing gain with increasing signal power emphasizes the fact that the VLFA should be placed at the proper location.

Figure 2(d) analyzes the gain characteristics of the VLFA with increasing erbium ion concentration. The figure shows that the gain of a 3.5-m VLFA pumped at 500 mW increases with increasing erbium ion concentration. As the erbium ion concentration increases from 0 to 9.0×10^{25} ions/m^3, the gain of the amplifier increases from -3.0 to 35.0 dB. Further increase in the concentration of erbium ions causes the gain to decrease.

Figure 2(e) shows the gain as a function of signal wavelength. This figure shows that the maximum gain achieved by a 3.5-m fiber pumped with a 500-mW excitation source and 9.0×10^{25} ions/m^3 erbium ion concentration is approximately 35.0 dB, at a signal wavelength of 545 nm. Although the emission cross section between the upper and lower lasing levels has a maximum at 553 nm [12], the ratio of the emission cross section to absorption cross section has its maximum at 545 nm [11]. Figure 2(e) proves that the gain is a strong function of the ratio of cross sections.

3.2. Noise Figure Analysis

The noise figure (NF) quantifies the noise characteristics of the VLFA and is defined as [17]

$$NF(dB) = OSNR(in) - OSNR(out) \tag{11}$$

where *OSNR*(*in*) and *OSNR*(*out*) are the optical signal-to-noise ratio at the input and the output respectively. NF can also be calculated from the amplified spontaneous emission P_{ASE} and gain G as follows [10].

$$NF = \frac{P_{ASE}}{h\nu\Delta\nu G} + \frac{1}{G} \tag{12}$$

P_{ASE} and G are functions of fiber length, pump power, concentration of erbium ions, and signal power. The amplified spontaneous emission power increases with increasing amplifier length; therefore, the noise figure of the amplifier also increases with increasing length. Figure 3(a) shows the noise figure as a function of fiber length at pump power of 400 mW, erbium ion concentration of 9×10^{25} ions/m^3 and input signal power of 1 μW. Figure 3(a) shows that the minimum noise figure is 3.15 dB. Under the given constant conditions, the noise figure increases from approximately 3.15 dB to 3.73 dB with increasing fiber length up to 2.5 m, and maintains a constant value of 3.73 dB for fibers longer than 2.5 m.

Figure 3(b) shows the noise figure as a function of pump power, keeping the erbium ion concentration at 9.0×10^{25} ions/m^3, input signal power at 1 μW, and fiber length at 3.5 m. The figure reveals that increasing pump power reduces the noise figure: When pump power increases from 0 to

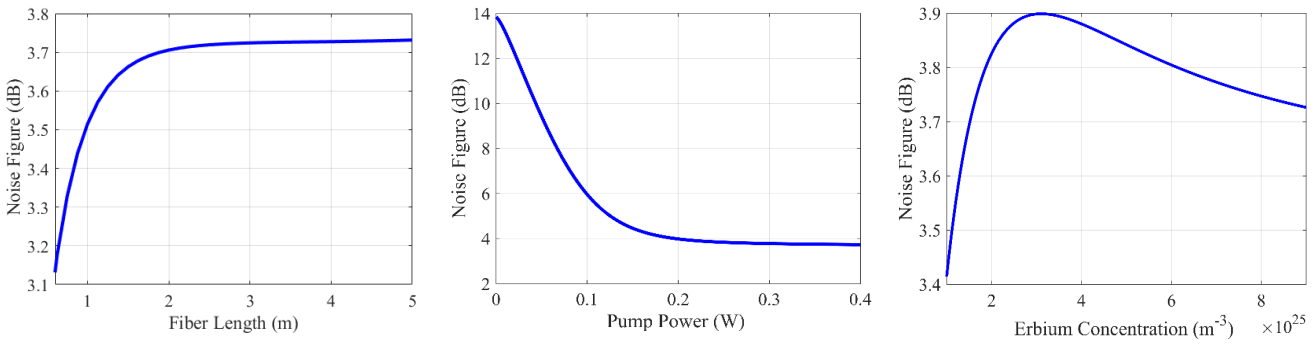

(a) (b) (c)

FIG. 3. Noise figure characteristics of the VLFA: (a) noise figure as a function of fiber length, (b) noise figure as a function of pump power, (c) noise figure as a function of active-ion concentration.

230 mW, the noise figure decreases from 13.1 to 3.73 dB. The noise figure of the amplifier remains constant for pump powers between 230 and 400 mW.

The increase in erbium ion concentration eases the amplified spontaneous emission of photons, which causes increase in the noise figure, as shown in Figure 3(c). The noise figure graph plotted against erbium ion concentration is calculated by keeping the pump power 400 mW, amplifier length 3.5 m and the input signal power 1 μW. It can be seen from the figure that when the erbium ion doping concentration increases from 1.0×10^{25} ions/m^3 to 3.0×10^{25} ions/m^3 the noise figure also increases 3.42 dB to 3.9 dB. The noise figure reduces for the erbium ion concentration more than 3.0×10^{25} ions/m^3 and maintains 3.73 dB minimum value.

IV. VLFA IN VLC

Figure 4 shows the block diagram of the proposed architecture of VLC under no-line-of-sight scenarios. The modulator modulates the input data and encodes it on top of illumination light for transmission. Under scenarios with no line of sight between transmitter and receiver, visible-light signals cannot be transmitted wirelessly. Wireless signals from the light source must be guided through a fiber, and the signal dissipates. To enable the visible-light signals to reach their destination meaningfully, VLFAs must be installed at the proper locations to amplify the dissipated signals. Finally, the receiver receives the data and decodes it as the output data.

The schematic diagram of the proposed architecture of VLC is shown in Fig. 5. Figure 5 illustrates that devices and users with possible line of sight (within the same room) can communicate wirelessly using a basic VLC architecture, but the devices under impossible line-of-sight scenarios (in different rooms) cannot communicate wirelessly. To enable the devices to transmit data beyond the line of sight, the visible-light signals must be guided through fibers, as shown with bold lines in Figure 5. As the visible-light signals will dissipate during transmission through a fiber, the optical amplifiers (VLFAs) must be installed at proper locations to amplify the dissipated signals and enable them to reach their destination.

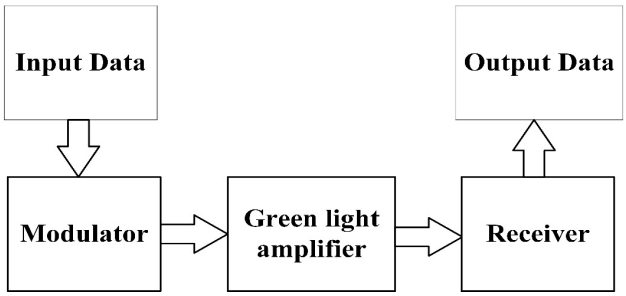

FIG. 4. Block diagram of the proposed novel architecture of VLC for no-line-of-sight scenarios.

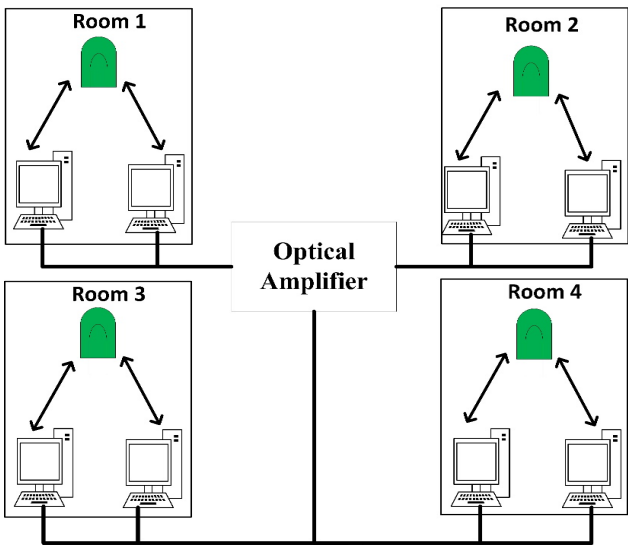

FIG. 5. Schematic diagram of the proposed model.

V. CONCLUSION

A visible-light fiber amplifier is modeled and analyzed mathematically. The numerical results show that a 3.5 m long silica fiber doped with 9.0×10^{25} ions/m^3 of erbium ions and pumped with a 500-mW excitation source can amplify green light from the visible spectrum, up to approximately 35.0 dB. Moreover, a numerical study of the noise figure characteristics of the amplifier reveals that the noise figure holds at 3.7 dB for amplifiers with fibers longer than 2.0 m, or pumped with more than 200 mW pump power. The constant value of the noise figure enables the VLFA to amplify the green signal without amplifying the noise further. The development of the VLFA and its application in VLC will make VLC more secure and extend the operating range of VLC, to completely replace rf systems.

REFERENCES

1. X. Dong, X. Cheng, H. Sun, and Y. Chu, "Scheduling with heterogeneous QoS provisioning for indoor visible-light communication," Curr. Opt. Photon. **2**, 39-46 (2018).
2. S.-M. Kim, "Visible light communication employing optical beamforming: A review," Curr. Opt. Photon. **2**, 308-314 (2018).
3. S. Vappangi and V. Mani, "Concurrent illumination and communication: A survey on visible light communication," Phys. Commun. **33**, 90-114 (2019).
4. F. Zafar, M. Bakaul, and R. Parthiban, "Laser-diode-based visible light communication: Toward gigabit class communication," IEEE Commun. Mag. **55**, 144-151 (2017).

5. M. Morales-Cespedes, M. C. Paredes-Paredes, A. G. Armada, and L. Vandendrope, "Aligning the light without channel state information for visible light communications," IEEE J. Sel. Areas Commun. **36**, 91-105 (2018).
6. H. Li, F. Wang, J. Zhang, and C. Liu, "Secrecy performance analysis of MISO visible light communication systems with spatial modulation," Digital Signal Process. **81**, 116-128 (2018).
7. R. Mulyawan, H. Chun, A. Gomez, S. Rajbhandari, G. Faulkner, P. P. Manousiadis, D. A. Vithanage, G. A. Turnbull, I. D. W. Samuel, S. Collins, and D. O'Brien, "MIMO visible light communications using a wide field-of-view fluorescent concentrator," IEEE Photon. Technol. Lett. **29**, 306-309 (2017).
8. Y. Xiang, M. Zhang, M. Kavehrad, and M. I. S. Chowdhury, "Human shadowing effect on indoor visible light communications channel characteristics," Opt. Eng. **53**, 086113 (2014).
9. W. A. Pisarski, J. Pisarska, R. Lisiecki, and W. Ryba-Romanowski, "Erbium-doped lead silicate glass for near-infrared emission and temperature-dependent up-conversion applications," Opto-Electron. Rev. **25**, 238-241 (2017).
10. P. C. Becker, N. A. Olsson, and J. R. Simpson, *Erbium-doped fiber amplifiers: fundamentals and technology* (Elsevier, 1999), Chapter 4-7.
11. W. J. Miniscalco, "Optical and electronic properties of rare earth ions in glasses," in *Rare-Earth-Doped Fiber Lasers and Amplifiers* (2nd ed.), M. J. F. Digonnet, ed. (New York: Marcel Dekker, 2001), pp. 17-112.
12. C. Jiang and L. Sun, "Gain characteristics of 980-nm pumped Er^{3+}-Tm^{3+}-Pr^{3+}-co-doped fiber," Appl. Phys. B **95**, 703-707 (2009).
13. K. Damak, E. Yousef, S. AlFaify, C. Russel, and R. Maalej, "Raman, green and infrared emission cross-sections of Er^{3+} doped TZPPN tellurite glass," Opt. Mater. Express **4**, 597-612 (2014).
14. E. Desurvire, J. R. Simpson, and P. C. Becker, "High-gain erbium-doped traveling-wave fiber Amplifier," Opt. Lett. **12**, 888-890 (1987).
15. F. Huang, X. Liu, L. Hu, and D. Chen "Spectroscopic properties and energy transfer Parameters of Er^{3+}-doped fluorozirconate and oxyfluoroaluminate glasses," Sci. Rep. **4**, 5053 (2014).
16. Y. Hu, S. Jiang, G. Sorbello, T. Luo, Y. Ding, B. Hwang, J. Kim, H. Seo, and N. Peyghambarian, "Numerical analyses of the population dynamics and determination of the upconversion coefficients in a new high erbium-doped tellurite glass," J. Opt. Soc. Am. B **18**, 1928-1934 (2001).
17. S. O. Kasap and R. K. Sinha, *Optoelectronics and photonics: principles and practices* (Prentice Hall New Jersey, USA), Chapter 4.